Scanning Early Data from the MINERνA Tracking Prototype

Colton D. O'Connor *College of William and Mary, Class of 2010*

Jeff Nelson *College of William and Mary, Dept. of Physics*

May 8, 2010

Contents

List of Figures

List of Tables

Abstract

MINERνA is a new neutrino experiment whose scintillator-based detector finished construction in March 2010. Data collected by this project will be crucial to the understanding of how neutrinos interact with matter and how they may be able to transition between flavors as they travel. By analyzing energy depositions, I characterize neutrino interactions recorded by a prototype of the detector. Events described include quasielastic interactions, resonant production of pions, and deep inelastic scattering. I also use simulations to investigate the physical responsivity of the detector to incoming particles and I am able to quantify the proportionality constants governing the fraction of ionizing energy that is visible to the data acquisition apparatus as a function of particle type and initial momentum.

1   Introduction

Much current research in the field of high-energy physics is devoted to increasing our knowledge of neutrinos, uncharged leptons with almost — but not quite — no mass. One such experiment is MINERνA (Main INjector ExpeRiment for ν-A), which was consciously designed in part as a companion to the MINOS (Main Injector Neutrino Oscillation Search) experiment. The Tracking Prototype, a subsection of the MINERνA detector, took its first data in the spring and summer of 2009. The neutrino interactions described by these data require careful analysis and categorization. The process of interpreting data is useful both as a way to benchmark event-categorizing software in development and as a way to enhance researchers' familiarity with the detector and the results it can produce.

2   History

The existence of neutrinos was postulated long before the Standard Model was developed. They were first proposed by Wolfgang Pauli in 1930 as a "desperate remedy" to the problem of missing energy in beta decay processes. It was not until 1953 that neutrino interactions were observed in a laboratory. The groundbreaking work of Cowan and Reines et al. was awarded a Nobel Prize four decades later.

Neutrinos are leptons, fundamental particles that do not interact by the strong force. They exist in at least three known generations (or "flavors" — much like quarks) named after their charged partner particles: the electron neutrino (ν_e), the muon neutrino (ν_μ), and the tau neutrino (ν_τ). The muon neutrino was observed in 1962 in an experiment which was later awarded a Nobel Prize; the tau neutrino was not observed until as recently as 2000. As their name suggests, neutrinos carry a neutral charge and so do not participate in electromagnetic interactions. At one time it was believed that they had zero mass, but evidence from the Super-Kamiokande (Super-K) experiment in Japan provided firm support for the theory that neutrinos oscillate between flavors over time — a theory that requires the particles to be massive. Nevertheless, they are the least massive of all known fundamental particles, with maximum masses summing to less than 1eV according to cosmological limits. Gravitational forces are negligible at subatomic distances (i.e., the scale of modern methods
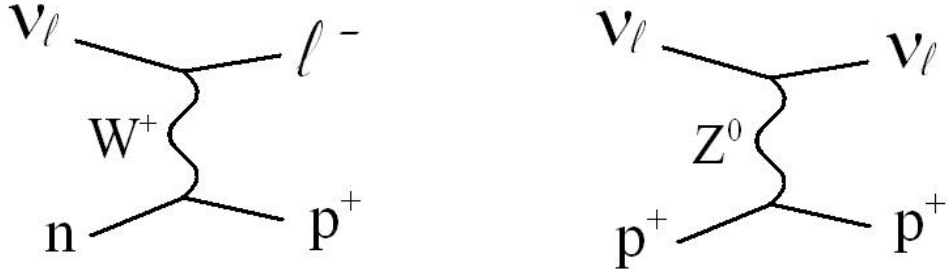
Figure 1: CC (left) and NC (right) neutrino-nucleon interactions mediated by the weak force.

of high-energy experimentation), so the weak force is the only means by which neutrinos interact in an observable way.

There are two main methods of interaction between a neutrino and a nucleon. In charged current (CC) interactions, a $W^{\pm}$ boson is exchanged with a nucleus to produce the charged lepton partner, e.g.:

$$\nu_\mu + n \rightarrow p^+ + \mu^- \tag{1}$$

In neutral current (NC) interactions, a Z^0 boson is exchanged as the neutrino scatters off a nucleon, e.g.:

$$\nu_\mu + p^+ \rightarrow p^+ + \nu_\mu \tag{2}$$

The Feynman diagrams are given in Figure 1. Neutrinos are the most numerous matter particles in the universe by a wide margin, but have very low probabilities of interacting. The mean free path of a neutrino in lead is about one lightyear, which is to say that a single neutrino would have to pass through a lightyear of pure lead to have a 50% chance of interacting with a nucleon at all. [5] On the other hand, an estimated 10^{14} neutrinos produced in the sun pass through each person on Earth every minute. [3]

Neutrinos that bombard Earth have three primary sources: the Big Bang, weak nuclear processes in the sun, and genesis through particle showers in the atmosphere incited by cosmic rays. Although neutrinos produced in the Big Bang are the most numerous, the are generally the least energetic and so the least likely to be detected. Recently, a great number of neutrino observatories have been constructed deep underground, to shield the
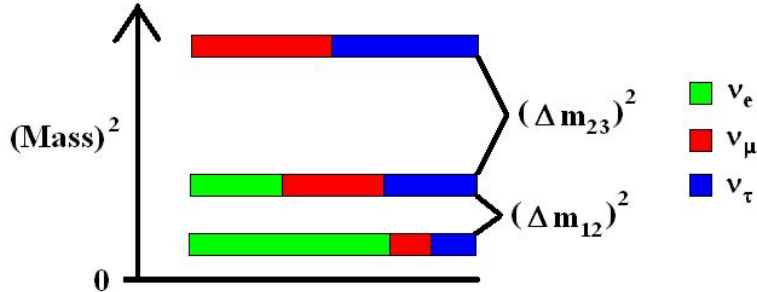
Figure 2: Neutrino mass eigenstates ν_1, ν_2, and ν_3, as combinations of the flavor eigenstates ν_e, ν_μ, and ν_τ. They are presented here in the "normal" hierarchy; an "inverted" hierarchy, placing ν_1 (and the smaller mass gap) at the top, is also possible.

detectors from cosmic rays. Some early findings in neutrino physics, however, were somewhat accidental. For instance, a range of studies on proton decay were being conducted in the 1980's that had to cope with significant background noise from atmospheric neutrinos. While Soudan 2 in Minnesota, the Kamioka Nucleon Decay Experiment (KamiokaNDE) in Japan, the Irvine-Michigan-Brookhaven (IMB) Experiment, and others did not detect proton decay, their results happened to shed great light on the $\nu_\mu \rightarrow \nu_\tau$ transition taking place as muon neutrinos in the atmosphere fell to the surface of Earth.

This flavor transition is by no means a trivial observation. The Standard Model initially assumed neutrinos to be massless and for decades there was no evidence to the contrary. However, there was no evidence precluding the attribution of very small masses to these uncharged leptons and in fact the mechanism of flavor-state oscillations requires it. According to the theory, neutrinos may be observed in three different flavor states and three different mass states, with each set of states forming a linearly independent basis capable of describing the particle. Thus, the lightest state is not simply the electron neutrino, but rather a linear combination of ν_e, ν_μ, and ν_τ quantum states. Only because neutrinos can be described in two distinct bases like this are oscillations between eigenstates possible. A visual depiction of the mass states, as combinations of flavor states, is given in Figure 2; a mathematical description is outlined by Equations 3 and 4.

$$|\nu_x\rangle = \sum_i U_{xi}|\nu_i\rangle \tag{3}$$

$$U = \begin{array}{c} \\ \nu_1 \\ \nu_2 \end{array} \begin{array}{cc} \nu_x & \nu_y \\ \begin{pmatrix} \cos\theta & \sin\theta \\ -\sin\theta & \cos\theta \end{pmatrix} \end{array} \qquad (4)$$

The elements of the matrix U in the Equations 3 and 4 refer to the so-called "mixing angle" that arises as an algebraic feature of the relationships between the two independent bases for describing neutrinos. The picture has been simplified here by showing the mathematical equivalence of flavor versus mass for describing two types of neutrinos; in reality, we must deal with a 3-by-3 matrix and three distinct mixing angles, as well as some hypothetical phase terms that arise if we allow neutrino oscillation processes to violate CP (the combination of Charge and Parity symmetries).

The current goal of many neutrino studies is to restrict the possible mixing angles and masses of the particles. This is accomplished indirectly by determining the rate at which each flavor oscillates into the others. In recent decades, the results available from many different experiments for comparison have greatly increased, with observatories in more than half a dozen countries across the globe. These investigations have varied widely in design. The Sudbury Neutrino Observatory (SNO) in Ontario, for instance, used 10,000 photomultiplier tubes (PMTs) to monitor interactions involving solar neutrinos in a 1-kiloton tub of heavy water. More recently, MINOS has made use of the 120-GeV Main Injector synchrotron proton accelerator at Fermilab in Chicago, bombarding a carbon target with 4×10^{20} protons per year in a pulsed beam. MINOS has "near" and "far" detectors, separated by 730 km of Earth's crust, which are used to compare the number of muon neutrinos in the beam at two points along its path, using a detector made up of thick planes of steel alternating with planes of scintillating plastic strips threaded with wavelength-shifting (WLS) fibers. MINOS was designed for finding neutrinos with a peak energy of 3 GeV.

One of the most important neutrino experiments to date has been Super-K, which preceded SNO by a few years using a similar set-up. Super-K was significant for being the first experiment to provide solid evidence of neutrino oscillations. The suggested probability,
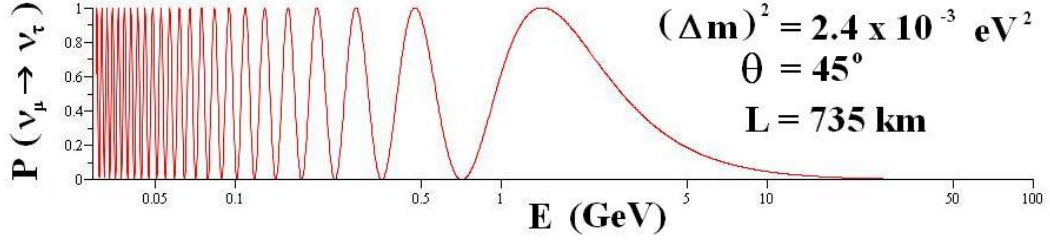
Figure 3: The probability shown here is that for mu-neutrinos oscillating to electron-neutrinos over the distance between the MINOS "near" and "far" detectors.

which first surfaced in the theory in the 1960's, is given below.

$$P(\nu_x \to \nu_y) = \sin^2(2\theta)\sin^2(1.27\Delta m^2 L/E) \qquad \{x,y\} \subset \{e,\mu,\tau\} \qquad (5)$$

The parameters L and E are derived from the particular experiment and represent, respectively, the distance traveled by the neutrino between its source and its detection in kilometers and the particle's energy in GeV. The values of the other parameters are not yet known; θ represents the mixing angle for a specific pair of neutrino flavors x and y, and Δm^2 is the difference between squares not of the masses of any mass states but of the expectation values of the masses of the flavor states between which the particle is oscillating, recorded in eV^2. The constant 1.27 falls out with this choice of units. Figure 3 shows that oscillation probabilities vary rapidly for low energies and less rapidly at higher energies.

If Δm^2 is less than 10^{-5} eV^2 or so, then the probability of oscillation will always be almost negligible. Experimental measurements have placed the likely values of both Δm^2_{12} and Δm^2_{23} between 10^{-5} eV^2 and 10^{-1} eV^2, representing a region in which the probability of oscillation depends significantly on the mixing angle and the value of L/E.

3   The Role of MINERνA

As explained, MINOS uses the Main Injector at Fermilab and observes neutrinos at "near" and "far" detectors. While MINOS is noteworthy for using the highest-luminosity beam available and for the great separation between source and final detection, its detection processes are in some ways coarse. For instance, experimental data from MINOS is not sufficient for the precise reconstruction of the total energy involved in neutrino interactions because final-state particles cannot always be identified. MINERνA was designed in part to make particle identifications clearer while providing fine measurements of the energies involved in certain interactions using a detector placed upstream of the MINOS "near" detector in the same beamline. Comparison of event images from the two experiments can reduce the systematic error in results from MINOS and other similar experiments.

Upstream of the MINOS and MINERνA detectors, the proton beam from the Main Injector first encounters a carbon target. Nuclear collisions produce a wide array of particles including charged pions that are directed toward the detectors by magnetic horns. En route, many of the pions decay into neutrino-lepton pairs. Those neutrinos emitted in the direction the pions are traveling make up the "neutrino beam" for MINOS, MINERνA, and other neighboring experiments. Most other particles produced along the way are removed from the beamline either by their own decay as the beam passes down the half-mile "decay pipe" or by interactions with matter as the beam is directed through a 200-m wall of solid earth.

Note that the beamline is not "left on" around the clock. Rather, the neutrino beam is delivered in brief "spills," each of which consists of about 3.4×10^{13} Protons (incident) On the Target, or POT. Any interactions resulting from a given spill are grouped together as a "gate." The reconstruction software is designed to isolate each event in the detector as a unique "slice" in time. Gates are further grouped into broader categories: sequentially-numbered "subruns" and overarching "runs."

On the other side of the rocks, the MINERνA detector itself meets the neutrino beam with an array of nuclear targets consisting of liquid helium, carbon, water, iron, and lead sheets. The purpose of the targets is to enable interactions between neutrinos and nuclei of various atomic masses. On the other side of the nuclear targets lie the "fully active" scin-

tillating hydrocarbon targets. The detector's core is surrounded and backed by electromagnetic calorimeters (ECALS) of lead and scintillator. The outermost and most downstream portions of the detector are the hadronic calorimeters (HCALs) of steel and scintillator. A schematic image is given in Figure 4.

The fully active core is constructed of individual strips of scintillator assembled into hexagonal planes, as shown in Figures 5 and 6. There are 200 planes, alternating between three orientations. Within each plane, triangular strips of plastic are assembled in an alternating tooth-up/tooth-down fashion so that the ratio of light scintillated in one strip to light scintillated in its neighbor by a single event can be used to determine the spatial position of any event to within 2.6mm in dimensions normal to the beamline. Along the beamline, spatial resolution is roughly 1.7cm, the thickness of each strip.

The full MINERνA detector now consists of 200 planes of scintillator, but it was only recently commissioned. A subset of the full detector known as the Tracking Prototype was assembled first for the purpose of taking preliminary data so that collaborators could begin data analysis, become accustomed to the form of the data, and modify procedures as needed in preparation for the completion of the detector. Twenty-four modules (each consisting of two planes) make up the Tracking Prototype, numbered based on their projected positions in the finished detector: modules 75-84 are layers of fully active core with lead sheets on the perimeter to act as side ECAL, modules 85-94 are alternating layers of scintillator and lead to serve as downstream ECAL, and modules 95-98 are interspersed steel and scintillator for HCAL.

Surrounding the planes, which constitute the Inner Detector (ID), are the "towers" that make up the Outer Detector (OD). Each tower consists of four pairs of scintillating plastic strips. The planes are inserted into steel frames — the light-blue regions in Figure 6. As that picture shows, these frames have slits into which the towers are inserted. Photons emitted by scintillation in both the ID and the OD are carried along wavelength-shifting fibers to photomultiplier tubes that record the activity.

While any activity generating charged particles can be seen by the MINERνA detector, three kinds of interactions will be of special interest. First, "quasielastic scattering" is a CC event wherein a neutrino scatters off a neutron such that a proton and a lepton
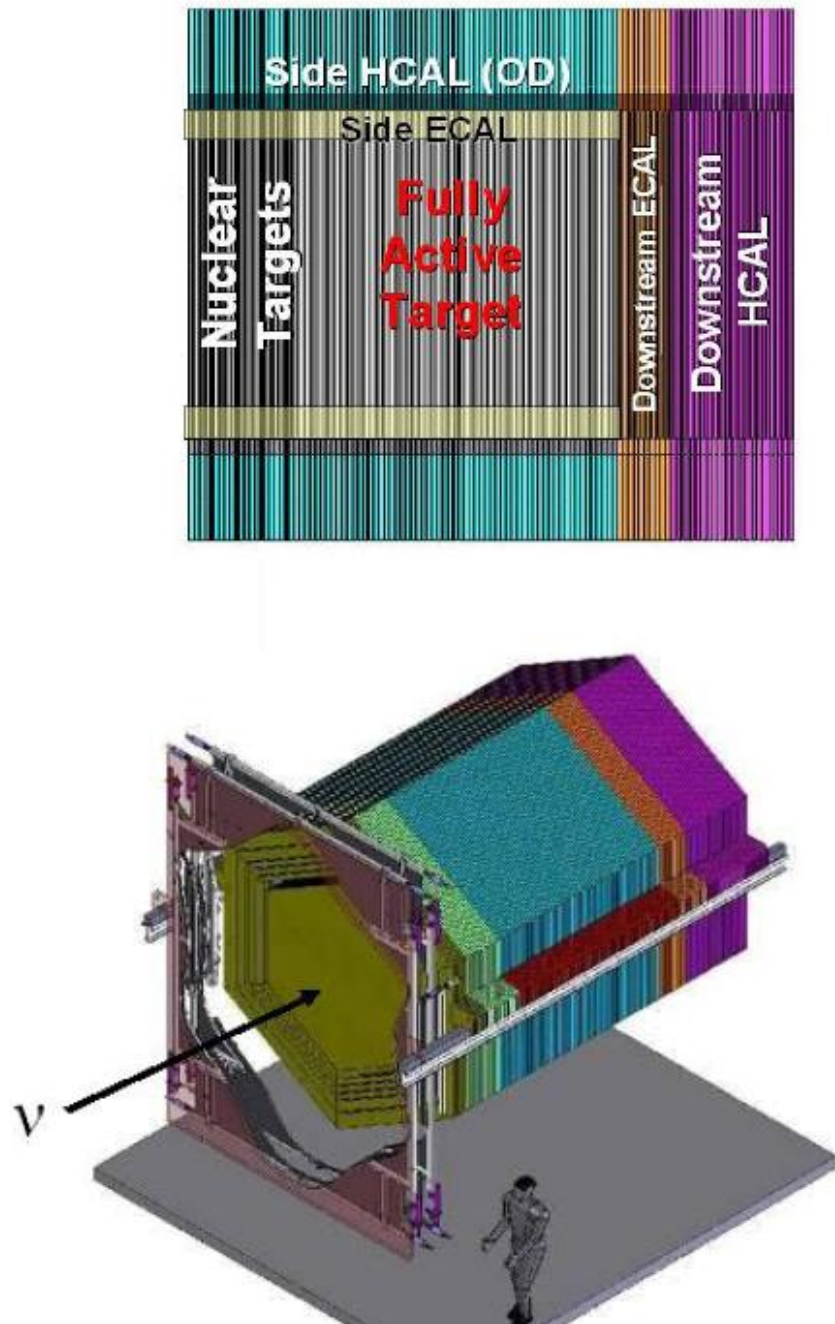
Figure 4: Two schematic views of the MINERνA detector, with a human figure for scale. [6]
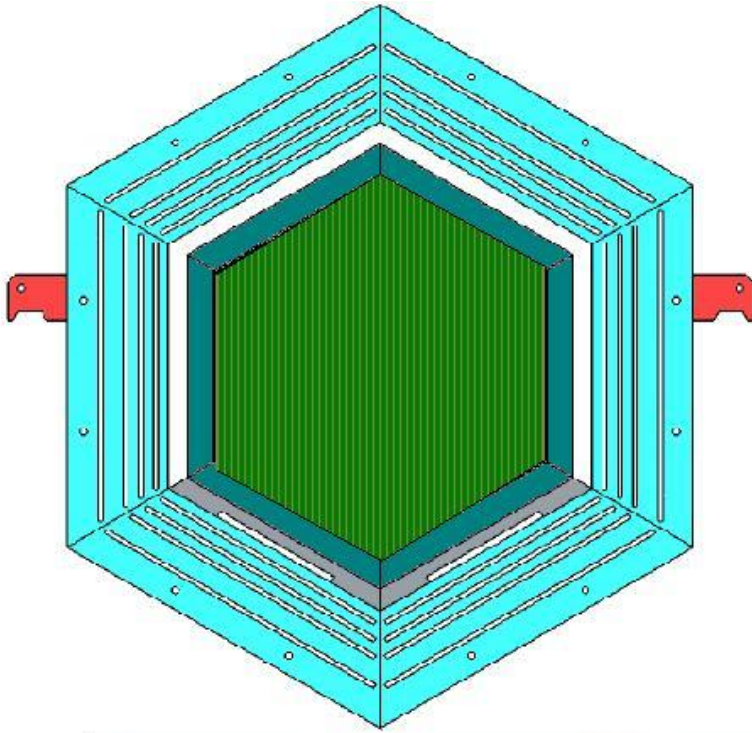
Figure 5: A beam's-eye view of an X-oriented inner detector plane. [6]
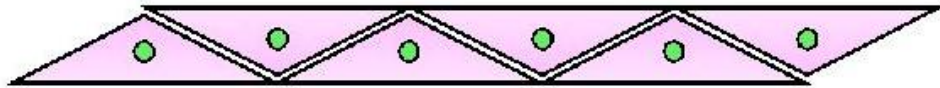
Figure 6: A depiction of the arrangement of the scintillating triangular strips that make up each plane, viewed from along the axis of the fibers threaded through. [6]
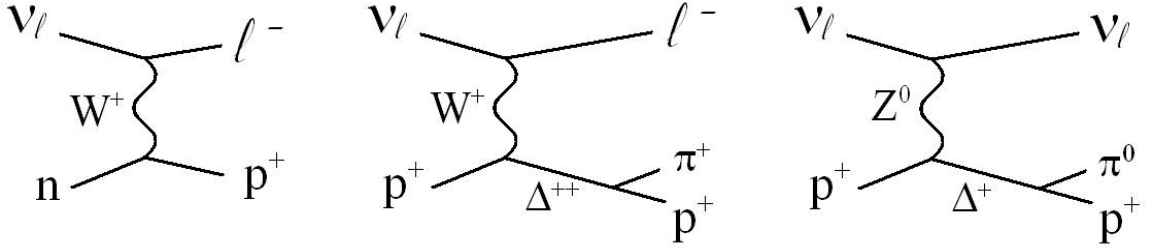
Figure 7: Quasielastic scattering (left) and resonance production (middle: CC, right: NC).

emerge. Second, "resonance production" refers to either a CC or an NC interaction which has a Δ baryon among its products. This will rapidly decay, resulting in a pion that may be neutral (π^0) or charged (π^+ or π^-). Feynman diagrams for these processes appear in Figure 7. Finally, "deep inelastic scattering" (DIS) occurs when a neutrino probes the internal structure of a nucleon. This quark-lepton interaction can have a large number of energetic products, often including multiple pions.

In reconstructions of MINOS events there is no way to determine how many particles of what kinds are produced during an interaction. Ionization energy losses can be used to determine the amount of kinetic energy involved, but particles are best identified by their distinct rest masses, which cannot be accessed by the MINOS detector. Currently, simulations are used to estimate the missing energies based on comparable data from older bubble chamber experiments.

MINERνA will be able to image all final-state particles following an interaction, and will provide enough supplementary information about incoming neutrino energies to greatly enhance the estimations of neutrino energies in MINOS. In tandem, the two experiments can provide better information for interpreting observations of neutrino oscillations, which should lead to greater knowledge of the mixing angles and mass differences.
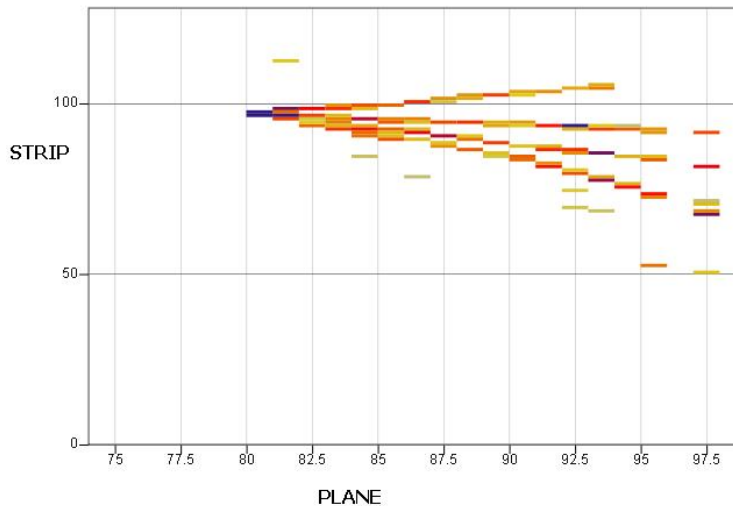
Figure 8: A CC neutrino event recorded by the MINERνA Tracking Prototype. Four daughter particles are evident. Average energy deposition per unit distance (dE/dx) is higher for blue points and lower for yellow points.

4 Tracking

Energy deposited in the fully active core of the MINERνA detector results in scintillation. Greater releases of energy will send stronger signals to the data acquisition apparatus so that the tracking data can also display the ionization ratio of each particle (in photoelectrons) as it traverses the detector. An example of such data is given in Figure 8. The geometry of the detector allows for three-dimensional mapping of each point at which a particle deposits energy — a process in which any charged particle with nonzero momentum participates continuously. These points are combined to reconstruct the trajectories of all charged particles in the detector. Particles entering the detector from the sides should be systematically ignored so that the only tracks presented in the data gathered are those representing particles produced in interactions between incoming neutrinos and nuclei within the detector.

One of the two primary physical means of energy deposition for charged particles in motion is ionization loss: the average energy loss dE by a charged particle due to ionization as it passes a distance dx through a medium. The path length is calculated in units of distance times density to indicate the amount of matter, and thus the number of nuclei,

11

traversed. The Bethe-Bloch formula for ionization loss is quoted here [7, p. 349].

$$\frac{dE}{dx} = \frac{4\pi N_A (z/e)^2 \alpha^2}{m_e v^2} \frac{Z}{A} \left\{ \ln \left[\frac{2 m_e v^2}{I(1 - \beta^2)} \right] - \beta^2 \right\} \tag{6}$$

Here, the speed and charge of the moving particle are v and z ($\beta = v/c$), the mass and charge of an electron are m_e and e, and the atomic number and mass number of the atoms in the medium are Z and A. N_A is Avagadro's number and α is the fine structure constant. I is an effective ionization potential for the atoms in the medium; since it is averaged over all electrons it can be cumbersome to calculate with precision but it usually suffices to approximate that $I = 10Z$ eV. Equation 6 has a modest dependence on the medium traversed, as Z/A is roughly 0.5 for all but hydrogen and the heaviest metals. With respect to ionization, then, the various regions of the detector shown in Figure 4 are indistinguishable.

The ionization energy loss for several singly-charged particles passing through a variety of solid, liquid, and gaseous media is depicted in Figure 9. There is a distinct minimum around $\beta\gamma = 3$ ($\gamma = [1 - (v^2/c^2)]^{-1/2}$ 10^2), below which the linear term of Equation 6 dominates and above which the logarithmic term dominates. Particles whose momenta correspond to that dip are called "minimum ionizing particles" (MIPs) and the region to the right of the minimum is referred to as the "relativistic rise." By contrast, dE is higher for lower-momentum particles, such as the sub-GeV protons that are sometimes seen by MINOS and MINERνA.

Secondly, energy is released by charged particles in the detector through *bremsstrahlung* radiation. Radiation energy loss is the physical motivation behind the materials used in constructing the ECAL. If a charged particle with energy E_0 enters a medium, its energy will decrease through radiation exponentially with the distance traversed, x.

$$E = E_0 \exp\left(-\frac{x}{X_0}\right) \tag{7}$$

The reference distance X_0 is known as the radiation length and is derived based on the probability of Coulomb scattering; the final form is given below for X_0 measured in cm$\times$(g/cm^3) [7, p. 353].
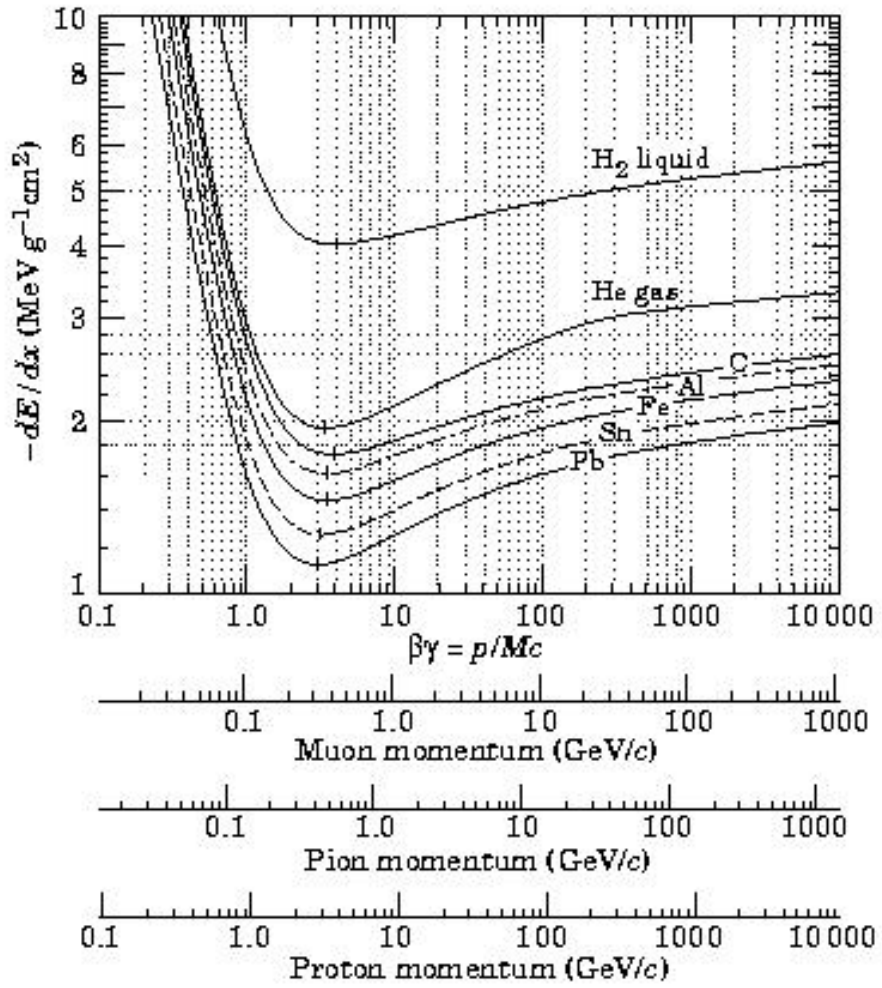
Figure 9: Graphical results of the Bethe-Bloch formula. [2]

$$\frac{1}{X_0} = 4Z^2 \left(\frac{N_A}{A}\right) \alpha^3 \left(\frac{\hbar c}{mc^2}\right)^2 \ln\left(\frac{183}{Z^{1/3}}\right) \tag{8}$$

Notice that the dependence on Z is far greater for radiative losses than for ionization losses. Taking advantage of this fact, the MINERνA Collaboration interspersed the layers (or "planes") of scintillator with 2-mm lead sheets (with a radiation length about one-seventh that of the scintillator) in the ECAL regions of the detector. These are meant to correspond to $0.57X_0$ for electrons and positrons. It is because of the mass dependence in Equation 8 that this form of energy deposition is significant for only the lightest leptons — for example, even muons would experience a radiation length 200 times larger than that experienced by electrons, reducing the sheet of lead from $0.57X_0$ to $< 0.001X_0$.

When a photon is emitted by *bremsstrahlung* radiation, it is likely to undergo pair production. Subsequent emission of photons by the daughter electron and positron create a cascade known as an electromagnetic shower. By imposing a material with shorter radiation length, the ECAL promotes these showers so that electrons and photons can be easily identified among daughter particles of neutrino interactions or subsequent decays. Crucially, a π^0 meson will rapidly decay into two photons, and, while both pions and photons are neutral and thus invisible to the detector, the leptons generated in the electromagnetic shower will leave distinct impressions in the data — compact regions of large light yields.

Eventually a shower will grow large enough that each lepton produced has too small a share of the total energy and will not radiate further. Once ionization losses become dominant, the number of particles in the shower will begin to dwindle as they are absorbed. Generally, in an electromagnetic shower's endgame, emitted electrons are absorbed through the photoelectric effect before they are able to pair produce. The full process of a shower takes a roughly ellipsoid shape in space as it grows and subsequently decays.

Despite a similar name, hadronic showers have a different way of propagating. These are started when an incident hadron collides inelastically with a nucleus and produces secondary hadrons. The second "generation" repeats this process with other nuclei downstream and so forth. Analogously to radiation lengths, we can refer to nuclear interaction lengths λ_0 for strongly interacting particles, approximated by Equation 9 for units of cm$\times$(g/cm^3).

	X_0 (g/cm^2)	λ_0 (g/cm^2)	Thickness in Detector
Scintillator (Polystyrene)	43.8	81.7	1.7 cm
Steel	13.8	132.1	2.54 cm
Lead	6.4	199.6	0.2 cm

Table 1: Radiation and Nuclear Interaction Lengths in MINERνA.

$$\lambda_0 \approx 35 A^{1/3} \tag{9}$$

Again, we see a more dynamic dependence on medium than for ionization losses. Hadronic showers are useful for identifying strongly interacting particles by their energy deposition; recall that ionization energy in the active scintillating planes between the steel is the only thing MINERνA actually sees. To promote showering, the HCAL is constructed with steel absorbers in between each layer of scintillator, each one 2.54 cm ($0.15\lambda_0$) thick. While sufficiently energetic muons will pass through the HCAL leaving only the distinct ionization trail of a MIP, hadrons will generally shower in one of the 20 steel sheets. Table 1 summarizes the properties discussed for the materials that make up the MINERνA detector.

5   Scanning

Energy deposited in the MINERνA detector by ionization is dependent on the momentum of the charged particle causing it. The presence of an electromagnetic or hadronic shower is indicative of particular species, whether muons, electrons, mesons, baryons, or photons. Combining all of this information, the data collected by MINERνA allows for the determination of what particles were produced in an neutrino interaction, where that interaction occurred, and what became of the products downstream.

Such analysis often requires subtle judgment and cannot yet be carried out by software alone. Computer-based processing will be necessary for the large amounts of data that will be gathered using the full detector once it is operational. Before that happens, the software must be benchmarked by comparing its results to human-eye analyses of the same samples using the relatively small batches of data from the Tracking Prototype.

I received training from Dr. Anthony Mann (Tufts University) in the practice of "scanning" data acquired by the detector such as that seen in Figure 8. This entails analyzing such an image visually and documenting key facts about it to be recorded in a project-wide database. Features of an event to be noted include the number of charged particle tracks originating at the primary vertex where the neutrino interaction took place, the ultimate fate of each of these daughter particles, and whether the image suggests any data acquisition problems in the electronics.

The full chart of input fields a scanner may utilize is shown in Figure 10. "ECAL events" are those whose primary vertex is within the ECAL; "rock" muons are those produced upstream of the detector and appear as single, straight tracks extending across and beyond the fiducial volume. Events flagged for detector problems may nonetheless be of interest and should be scanned, whereas unanalyzable events are those of which no useful sense can be made. The "vertex activity" field counts both the primary vertex if it is hot and signals near the vertex if they do not qualify as anything else. Shower prongs are particle tracks that shower in the ECAL or HCAL; track prongs are particles that do not. Tracks are numbered in clockwise order, starting from 12 o'clock.

A particle produced by a neutrino interaction may experience any of several predefined

Figure 10: The standard fields of information available to be filled by a scanner as needed for each event.

fates: the radio buttons in Figure 10. Some of these are easy to diagnose: a secondary scatter downstream is identified by a marked angular deflection in the track, while an electromagnetic shower has a shape similar to an ellipsoid in space. However, other options can be mistaken for one another. Consider the two tracks in Figure 11. The right edge of the graph represents the rear of the detector, while the sides of the detector are the top and bottom of the graph. But this graph is two-dimensional, and fails to express the other sides of the detector that are in front of and behind the plane of the image.

To remedy this ambiguity, strips in the planes of scintillator in the MINERνA detector bear three distinct orientations, along axes dubbed X, U, and V. The U- and V-axes are at 60° to the X-axis on either side of it. Twice as many scintillator planes bear the X-orientation as bear either of the others, so this is the most commonly referenced view and the one that appears in, for instance, Figure 11. However, the others are available for every event, and a three-dimensional topology can be reconstructed from such data as is seen for the same interaction in Figure 12. A comparison of all three views is enough to ensure the scanner that neither track exits the three-dimensional surface that is the side of the detector. The first (higher) track can be seen to certainly exit the rear of the detector,
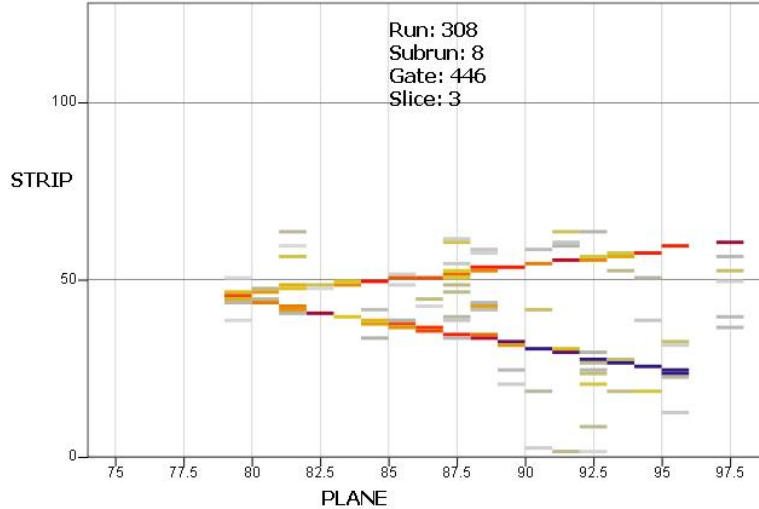
17

Figure 11: A neutrino event that may be a quasielastic interaction as described in Figure 7.

while the second (lower) track evidentially stops — or "ranges out" — within the fiducial volume. The six smaller views in Figure 12 show energy deposition in the towers.

While shower prongs and track prongs emerge from the primary vertex, which must be identified by the scanner, secondary vertices may appear downstream. These generally represent interactions involving uncharged (and thus non-ionizing) particles generated at the primary vertex that were invisible to the detector, but the products of whose interactions are charged and leave clear trails. Shower tracks that appear in the ECAL and appear to point back toward the primary vertex are signs of photons (called "gammas" in Figure 10). Pairs of photons often indicate the production of a π^0 particle at the primary vertex that rapidly decayed. Secondary vertices whose products fly off in a distinct V-shaped topology are taken to be downstream decays of strange particles such as Kaons or Λ baryons. Odd tracks that appear downstream and do not exhibit "pointing" toward the primary vertex are assumed to be generated by collisions of neutrons (generated by the neutrino event) with stationary nuclei. As I illustrate my description with examples, it should be noted that all event data I have examined has been collected by the Tracking Prototype.

Some events — unfortunately, rare ones — are very clear in terms of what they depict. For instance, consider Figure 8. It would be the job of a scanner such as myself to identify that the vertex is hot, that there are four track prongs, that the first of these ranges to a
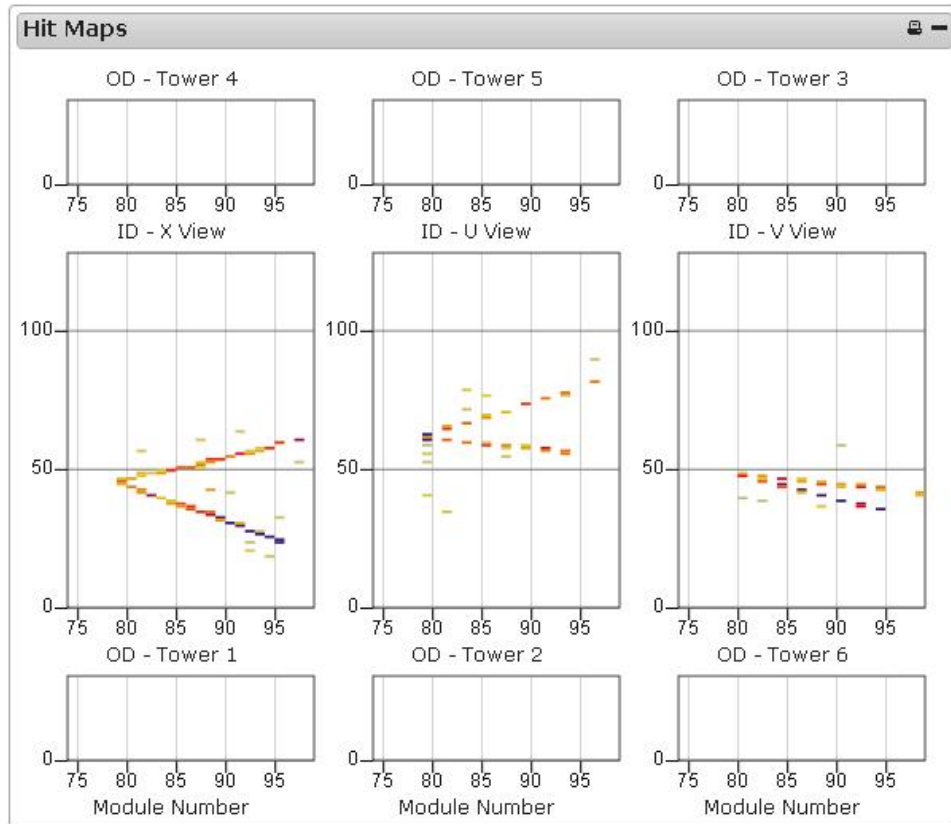
Figure 12: Multiple views of the event seen in Figure 11 representing the X-, U-, and V-orientations.

Data Type	Number of Examples	Percent
No Data	62	31%
Noise Only	45	22.5%
Outer Detector Activity	40	20%
Rock Muon Present	39	19.5%
Neutrino Event Outside of Fiducial Volume	13	6.5%
Analyzable Event (1 Prong)	5	2.5%
Analyzable Event (2 Prongs)	4	2%
Analyzable Event (3 Prongs)	1	0.5%
Analyzable Event (More Than 3 Prongs)	1	0.5%
Analyzable Event (Shower Present)	3	1.5%

Table 2: Frequency of various data types in the Tracking Prototype, based on a survey of 200 slices. The rightmost column refers to the percentage of those 200 slices displaying each particular data type.

stop, and that the other three all exit out the rear of the detector. A scanner is not expected to deduce that the first track represents a muon or that the other three represent positively-charged pions. Those are judgments left to specialists that will be more important later in the course of the MINERνA project. For the moment, the crucial facts are regarding what the daughter particles do, not what they are. The Tracking Prototype's thin rear HCAL is responsible for the ambiguity that should be in large part cleared up in data from the full detector.

To give some impression of just how infrequent interesting events truly are, I conducted a survey of 200 slices (see Section 3) of data taken with the Tracking Prototype. I arbitrarily selected to analyze Run 597, Subrun 17, Gates 100 through 162. Consult Table 2 to see what types of data was present in what proportions. Note that categories in the table are not mutually exclusive, with the exceptions of No Data and of Noise Only. In particular, Outer Detector Activity can occur either alone or in conjunction with activity of any type in the Inner Detector; and analyzable showers, being prongs themselves, will always cooccur with at least one prong. The No Data category tracks the fact that the final slice of each gate contains no hits, real or artificial, simply due to the fact that the gate does not close until some time after the final content-bearing slice has closed.

To become a qualified scanner, I had to pass a series of tests. Each of these consisted of a set of events of varied form and quality that I was asked to scan. Collaborators had

already compiled consensus descriptions of all test events which were held as standards against which my submissions would be compared. If my characterizations agreed to a high degree with those of the specialists, then I passed the test. After more than 100 test events, I received notification that I was a certified scanner and was eligible to participate in the ongoing General Scan and any subsequent projects. The General Scan was a landmark effort in neutrino physics, described by Dr. Mann as "the first time... that a sizable sample of images recorded by a high-resolution particle detector has been manually scanned by a globally distributed team of experimentalists using web-based software."

5.1   Characteristic Footprints of Critical Particles

As an extension of the basic task of a scanner, some particles can indeed be readily distinguished by the characteristic energy deposition patterns they yield. For instance, prongs that begin in the tracker region and pass through the ECAL and HCAL to exit out the rear while releasing a fairly constant and low amount of ionizing energy represent MIPs. Such a particle is probably either a muon or a charged pion.

Protons produced by neutrino interactions in the detector are typically not fully relativistic, i.e., their rest energy is comparable to their kinetic energy. Since they therefore lie on the steep slope on the left side of Figure 9, they tend to slow down rapidly, releasing more ionizing energy as they go and ultimately "burning out" after leaving only a very short track. Hadrons with greater kinetic energy will typically shower in the HCAL region. This includes some protons, π mesons, and others. Because the Tracking Prototype incorporates few HCAL modules, these events are not yet well documented.

The ECAL is where light electromagnetic particles can be best identified. Electrons and photons will shower in this region while other particles usually will not. However, the shape of the showers generated by these two particle types is the same, except that the vertex of an electron shower will be connected to a visible track from the primary vertex while that of a photon shower will not. It is well known that π^0 mesons, when produced in the detector, will decay rapidly to two photons. Since this particular decay process is the only likely source of high-energy photons in MINERνA, pairs of ECAL showers can be assumed to be from photons (also called "gammas" or γ particles) while events with only one ECAL

shower probably involve an electron.

Figure 10 contains a field for K^0/Λ decays because these are identifiable by their "V" shape. That "V" is oriented coaxially with the incoming neutrino beam, such that its vertex will be on the left and it will open to the right on the MINERνA event displays. There is another field for neutrons, which appear only rarely but leave a unique energy deposition pattern. Electrically neutral and thus non-ionizing according to the Bethe-Bloch formula, neutrons produced by a neutrino interaction remain invisible to the detector while experiencing typically several downstream collisions. Any such collisions that produce new particles will show up as a so-called "neutron star," a small-area burst of energy. Other particles produced by a neutrino interaction in the detector will leave linear (or slightly curved) paths that trace back to the vertex at which they originated; neutrons are generally recognizable because their footprints do not point back to the primary vertex and in fact may not even appear prong-shaped.

5.2 Illustrative Examples

It may be useful to demonstrate the appearances of certain interaction types or topologies. Figure 13 records a neutrino interaction that generated one particle that experienced a downstream scatter, giving its track a distinct kink, and one π^0 meson, identifiable by the pair of photons that remained invisible to the detector until they initiated electromagnetic showers in the ECAL. While the exact identity of the particle that scatters downstream is difficult to determine by inspection alone (and would likely be guessed at only with reference to branching ratios), its relatively low-energy track shows it to be a potential MIP.

For another example, consider Figure 14, which may be a candidate for a deep inelastic scattering interaction. The profusion of particles visibly produced by this rare nuclear interaction may have resulted in disruptive amounts of energy deposition, enough to cause detector problems resulting in a loss of data at certain points. The important facts for a scanner to log would be the large amount of energy present at the clear primary vertex and a guess as to how many prongs their are and what their fates are. I would analyze Figure 14 as depicting five prongs, the first and third of which (counting clockwise from 12 o'clock) shower in the ECAL just after plane 85, the second and fourth of which exit out the rear of
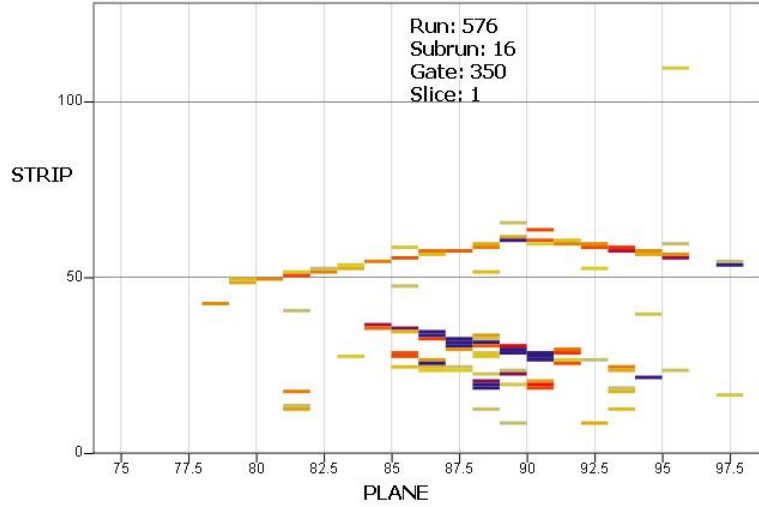
Figure 13: A neutrino interaction with multiple products.

the detector, and the fifth of which ranges to a stop with its last clear hit being at plane 93. The U- and V-views may help a scanner in working out such an analysis, though in cases such as this one those views are often just as difficult to distinguish as the X-view is.

Sample events such as these are used to benchmark the automatic analysis software that will be employed for scanning data from the completed detector. The goal is for the software in development to agree with human scanners about the nature of interactions in MINERνA and the particles involved.

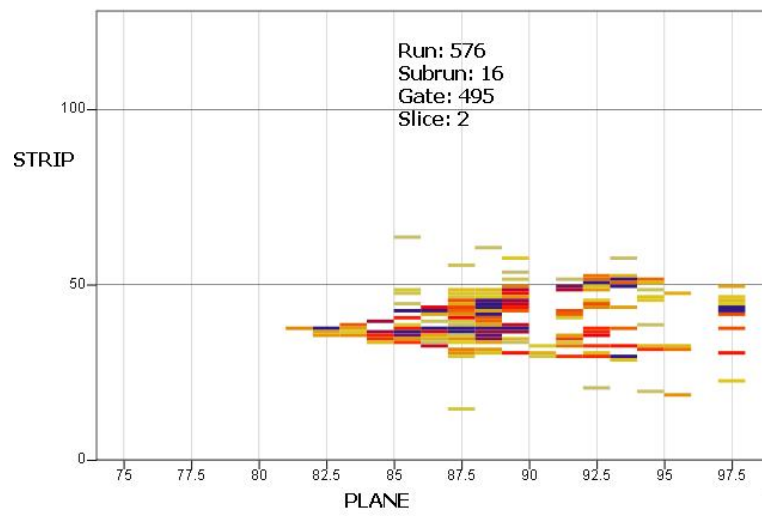Figure 14: The apparent corruption of the data represented by the gaps or "holes" is not a reason to ignore this interesting interaction.
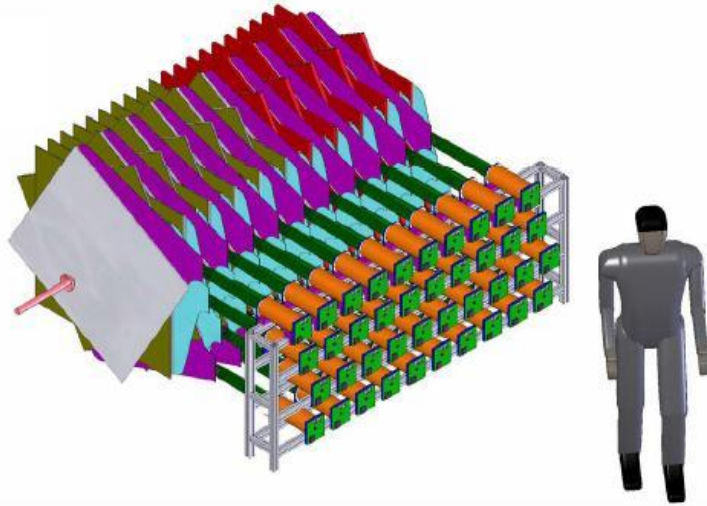
Figure 15: Schematic drawing of the MTest detector with all planes hung and photomultiplier tubes attached, with a human figure for scale. [6]

6   MTest Detector

In addition to the above work with the MINERνA Tracking Prototype, I have contributed to the efforts on the MINERνA Meson Test Beam (MTest) detector. In many ways, the MTest side project is like a scaled-down version of MINERνA used for calibration and for benchmarking simulation efforts. The detector will consist of 40 rectangular planes, each 1.07 m $\times$ 1.07 m, constructed from triangular strips of scintillating plastic in the same manner as the larger MINERνA inner detector planes with PVC frames around all four sides. Like those in the MINERνA inner detector, the planes will be hung alternating between three orientations labeled X, U, and V. Wavelength-shifting optical fibers are routed through each strip and guided to photomultiplier tubes by a snout in the frame to carry information about energy deposited in the detector. A full schematic of the MTest detector is shown in Figure 15.

Just as the MINERνA inner detector has tracker, ECAL, and HCAL regions, so too will the MTest detector. However, the design of the MTest detector is versatile, allowing that the lead and steel planes associated, respectively, with the ECAL and HCAL regions can be reorganized in between data collection runs. In this way, data can be collected from the MTest beam using a variety of detector configurations: some of those planned include 16

planes of tracker, 20 planes of ECAL, 4 planes of HCAL (mimicking the Tracking Prototype); and 8 planes tracker, 0 planes ECAL, 32 planes HCAL (for a focus on hadronic calorimetry).

The goals for the MTest investigation are to use an incident beam of identified particles of known momentum and measure the detector's response in terms of the visible energy deposited in each region. In preparation for a full analysis of data from the MINERνA detector, the project's simulations must be refined with better information about the responsiveness of each region of the detector to many particles, such as protons that range to a stop in the tracker, or charged pions that enter the HCAL. In particular, the MTest investigation will study the visible signs in the detector of a particle that enters from the front rather than being generated by a neutrino interaction within the fiducial volume of the detector itself. That is, the MTest beam will not be a neutrino beam like that used for MINERνA, but rather a beam of mostly protons, pions, and muons.

Ideally, the information yielded by the MTest detector as a particle enters in and either ranges or interacts within the detector should be enough for the initial energy of the particle to be reconstructed. Just as important is the identification of patterns of hits associated with different particle types (e.g., how far does an electron shower spread out laterally?) By using particles of known initial energies and measuring the total response in the MTest detector while visually checking the distributions of energy deposition, we can test the success rate of our identification methods. The lessons learned from the MTest beam will be applied first to simulations of the MINERνA detector's response to various particles and interactions and second to analysis of the data actually gathered by the detector.

6.1   Source Testing

One of my roles was to design and implement a quality assurance procedure for determining the responsiveness to ionizing radiation of the MTest planes constructed at the College of William and Mary before they were delivered to the installation site. I mapped a grid of 24 test points onto the face of each plane with spacing between points easy to locate relative to the structure of its PVC frame. Figure 16 shows the positions of these test points relative to the body of a plane.

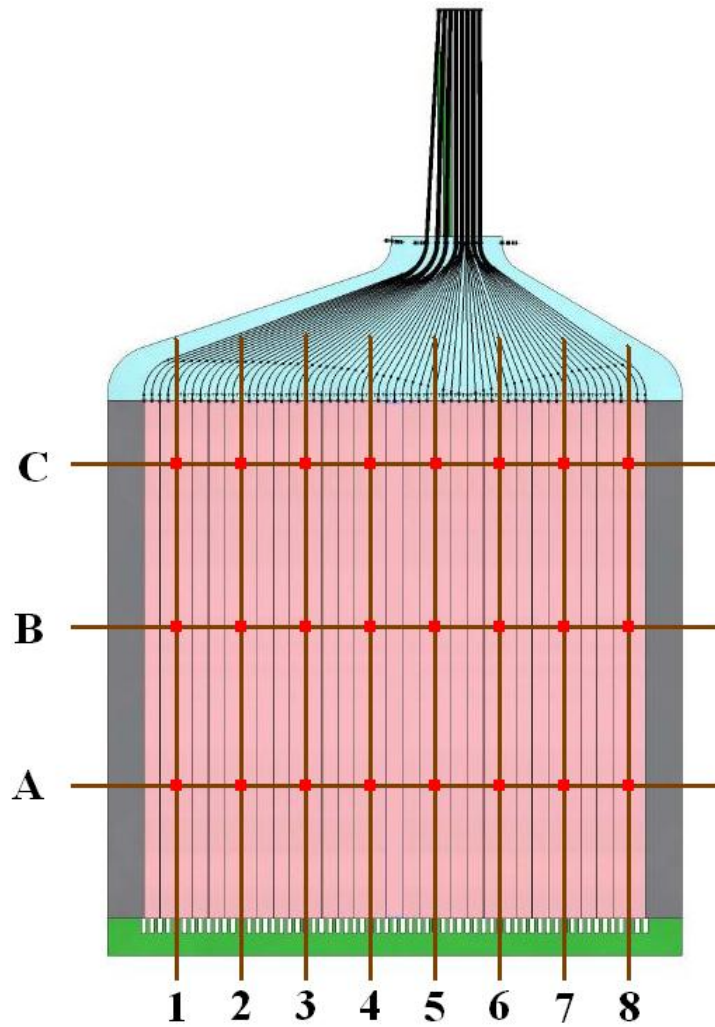During testing, the optical fibers of the plane were attached to a photomultiplier tube

Figure 16: Schematic drawing of an MTest plane (X-orientation) with a superimposed grid showing the positions of points where the source was placed during quality assurance testing as red squares.

read out on a picoammeter while a 40-μCi sodium-22 gamma source was placed four inches above the plane (using a simple styrofoam fixture) directly over each test point in succession. An MTest plane consists of 63 scintillating strips whose fibers are grouped into seven bunches of eight and one bunch of seven. Therefore it was necessary to record data with the source placed above each grid point eight times — once while each bunch of fibers was attached to the photomultiplier tube. In practice, some of the data became apparently redundant, so that 25% of the total test points for each plane were systematically skipped. This was a time-saving concession to the needs for the source testing process to be conducted by hand and for the planes to be shipped out on a frequent basis.

My formal involvement in the source testing effort ended shortly after I standardized the methods when the fourth plane constructed at the College of William and Mary was shipped to Fermilab. Those first few planes were all similar in their acceptable levels of responsiveness. As of the end of April 2010, the construction of the intended 40 MTest planes is nearing completion.
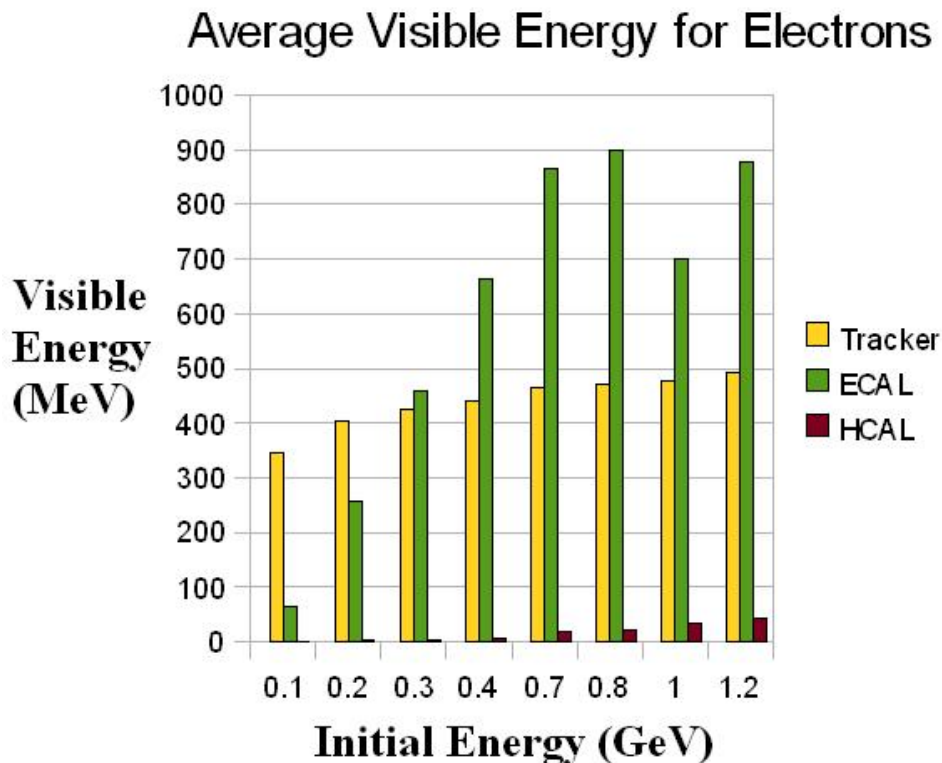
Figure 17: Average amounts of visible energy in the tracker, ECAL, and HCAL regions of the MTest detector as deposited by incoming electrons.

7   Simulation-Based Analysis of Visible Energy

Large numbers of events in the MTest detector can be simulated in order to answer physics questions. The simulated data themselves, along with the results of such an investigation, can then be compared against actual data obtained when the MTest beam is turned on. Most of these simulations use a model in which the detector is arranged like a miniature Tracking Prototype: 16 forward planes of tracker, 20 planes of ECAL, and 4 rear planes of HCAL.

As an introduction to a simulation-based analysis I have conducted, consider Figure 17, which shows values for the visible energy in each section of the MTest detector deposited by electrons with various initial energies (shown along the x-axis). Each value in Figure 17 is an average computed over a run of 1000 simulated events featuring electrons entering the MTest detector with the indicated energy.

Notice that low-energy electrons tend to burn out in the tracker region while ECAL showers dominate above 0.3 GeV. Only a small amount of energy ever appears in the HCAL, although from the plateaus in visible energy in each region one might suggest that electrons above 1.0 GeV occasionally produce showers whose final products escape out the rear of the detector.

A naive view might suspect that a simple linear relationship could hold between the total energy deposited in the MINERνA detector and the amount of light detected. The light is produced by ionization in the scintillator, which represents the same basic physical process at all points, so there might be a simple proportionality constant for the fraction of the total deposited energy that is visible to the hardware. This is a helpful perspective and, although some significant corrections apply, it can lead us toward an interesting and useful analysis.

First, it must be realized that each section of the detector will be characterized by a different coefficient. Since the fully active tracker has almost its full mass in scintillating plastic, it should register a fairly high portion of the ionization energy — hence, "fully active." The ECAL region contains alternating planes of lead and scintillator. None of the energy deposited in the lead will be visible to the detector, so a smaller percentage of the deposited energy will be visible. By the same reasoning, the thick steel planes of the HCAL will render invisible much of the ionization energy in that region. So we can speak of three proportionality constants for the three parts of the detector: let us call them A for the tracker, B for the ECAL, and C for the HCAL.

Second, different particles behave differently. The rate of ionization by an electron is not the same as that of ionization by a muon at the same energy. Momentum is the crucial parameter. In fact, dE/dx for a high-momentum muon will not be identical to that for a low-momentum muon, which is clear from the very existence of the curve in Figure 9. So, we have coefficents such as $A_{electron,0.8GeV}$ and $B_{muon,1.2GeV}$. While it is difficult to predict precisely how the correspondence between total deposited energy and visible energy will vary with particle type and momentum, we can assume that in each case the relationship will remain linear. This certainly merits some investigation.

To study the matter, I composed a ROOT script [8] that would analyze runs of 1000

simulated events in the MTest detector. Within a given run, all 1000 events represented the same particle entering the MTest detector with the same initial energy.

Initially in the analysis of a given run, reasonable seed values must be obtained for each of the three coefficients particular to the particle and momentum simulated. My approach was to set up linear systems, solving for A, B, and C by using the known value for total energy deposited and the sum of the visible energy in each of the three regions in each event. This method only works for the special case when the energy of the simulated particle is totally contained within the detector (i.e., that the simulated particle did not exit out the rear of the MTest detector) such that the total energy deposited is equal to the pre-set energy value selected for the run. This constrained which particle types and momenta could be used. The basic linear algebraic method for analyzable cases is depicted below.

$$
\begin{aligned}
E_{1,tracker}A &+& E_{1,ECAL}B &+& E_{1,HCAL}C &=& W_1 \\
E_{2,tracker}A &+& E_{2,ECAL}B &+& E_{2,HCAL}C &=& W_2 \\
E_{3,tracker}A &+& E_{3,ECAL}B &+& E_{3,HCAL}C &=& W_3
\end{aligned}
\tag{10}
$$

Here, $E_{i,x}$ represents the visible energy deposited in region x for event i while W_i is the total energy deposited in the detector for that event. Such a system of equations is solved by simple matrix methods to yield a value for each A, B, and C. From a run of 1000 events, many such systems can be obtained. Ideally this process should give 333 values for each of the coefficients (with one odd-man event left out at random), but in practice some of the systems prove insoluble due to oddities in the simulated event such as the generation of an additional particle. In any case, as many systems as possible are solved to produce a distribution of values for each of the coefficients. The mean of each distribution is taken as the seed value A_0, B_0, or C_0.

Once seeds are obtained, these estimates of the coefficients associated with a given particle of a given initial energy can be improved through iteration. To iterate a single variable, my approach was to hold the other two constant and determine what value of the focused variable would be necessary to properly account for the invisible energy in each event. That is, using known constant values for, e.g., B_0 and C_0, I search for the improved estimate A_1 by solving

$$E_{i,tracker}A_1 + E_{i,ECAL}B_0 + E_{i,HCAL}C_0 = W_i \qquad (11)$$

for $1 \leq i \leq 1000$. Currently, my approach is to iterate each of the coefficients in turn three times. Including the initial pass for obtaining seed values, this requires reading through each event in a run ten times. Note that the iterative process fundamentally differs from the algebraic technique so that the distributions of values obtained from the latter are not directly comparable to those derived from the former.

Some results can be seen in Figure 18 for a run of electron events with a total deposited energy of 0.4GeV. The distributions for A and B appear to have narrow peaks while the distribution for C has a much greater variance. This is largely due to the fact that not all simulated particles penetrate as far as the HCAL, and those that do may vary widely in the remaining energy they carry when they reach that region based on the length and shape of the path they have taken to that point. Furthermore, the relative "hairiness" of the plots corresponds well with the number of planes associated with each region: 16 tracker, 20 ECAL, and only 4 HCAL. Fewer planes lead to coarser data.

To decide, however, whether results that visually appear clean are in fact good representations of the effects at play in the data, we can consider whether the change in the mean value of each coefficient over any given iteration was large. Table 3 shows how A_i, B_i, and C_i related to A_{i+1}, B_{i+1}, and C_{i+1} for the same run (0.4-GeV electrons). While the first changes in the tracker and HCAL coefficients may be substantial, all three coefficients undergo only small changes in the second and third iterations. It is also promising that the change in A over multiple iterations is not monotonic. These are probably signs of the coefficients being close to their "true" values, which should represent equilibria in this iterative approach.

Since the coefficient values obtained in this way are only useful in the case of total energy containment — no particles from the event escaping from the detector — this process could only be carried out accurately up to a certain maximum initial energy for any given particle. As a test, coefficients were calculated for electrons for a sampling of initial energy values (not evenly spaced) ranging from 0.1 GeV to 1.2 GeV, with C being fixed to zero in all cases.
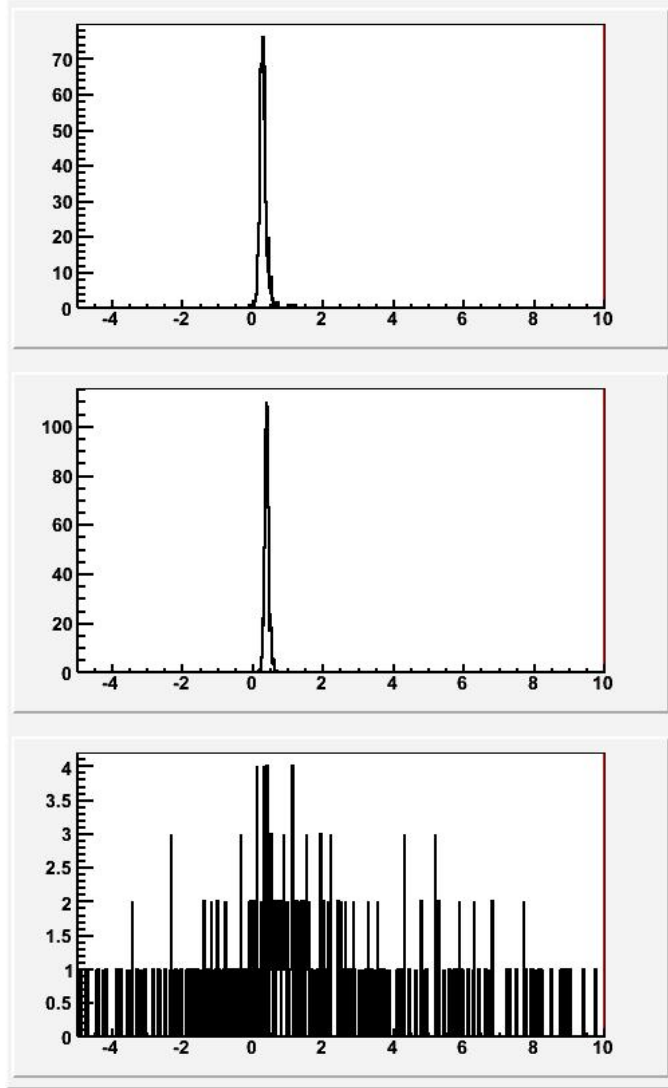
Figure 18: Distributions for $A_{electron,0.4GeV}$ (top), $B_{electron,0.4GeV}$ (middle), and $C_{electron,0.4GeV}$ (bottom).

	A	B	C
Seed Value	0.38	0.41	1.26
1st Iteration	-25%	-1%	+13%
2nd Iteration	0%	-1%	+3%
3rd Iteration	+2%	-1%	+6%
Final Value	0.29	0.40	1.56

Table 3: Fluctuation in $A_{electron,0.4GeV}$, $B_{electron,0.4GeV}$, and $C_{electron,0.4GeV}$ over three iterations.
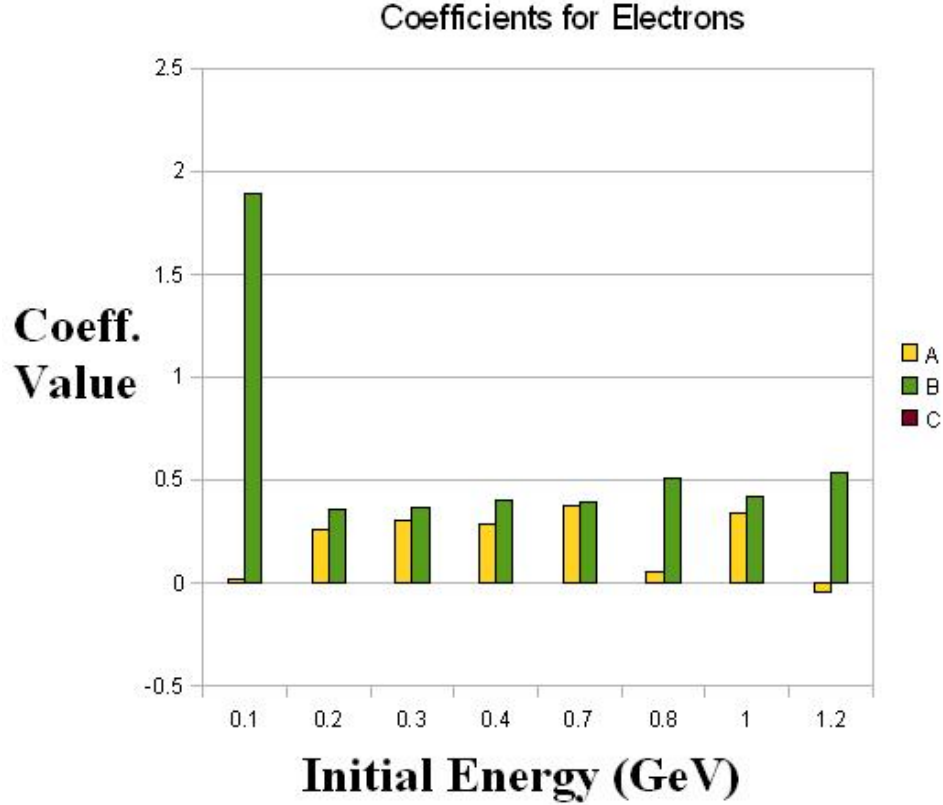
Figure 19: Final values for $A_{electron}$, $B_{electron}$, and $C_{electron}$ at various energies after three iterations.

Holding C at zero treats the rare instances of energy deposited in the HCAL as unimportant so that sparse fluctuations in the development of electromagnetic showers do not have a large effect on the values of all three coefficients. The results are shown in Figure 19. Previously, Figure 17 was used to approximate at what point energy from electrons began to exit out the rear of the detector. Now another method can be used: the coefficients in Figure 19 can be respectively multiplied by the average visible energies in Figure 17 and then the products summed to yield values for the total reconstructed energy. This has been done in Figure 20.

Evidently the coefficients calculated with C fixed at zero were adequate to accurately reconstruct energies up to 0.4 GeV, but not those at or above 0.7 GeV. This indicates that significant amounts of energy begin to appear in the HCAL for electrons with momenta at least that high.
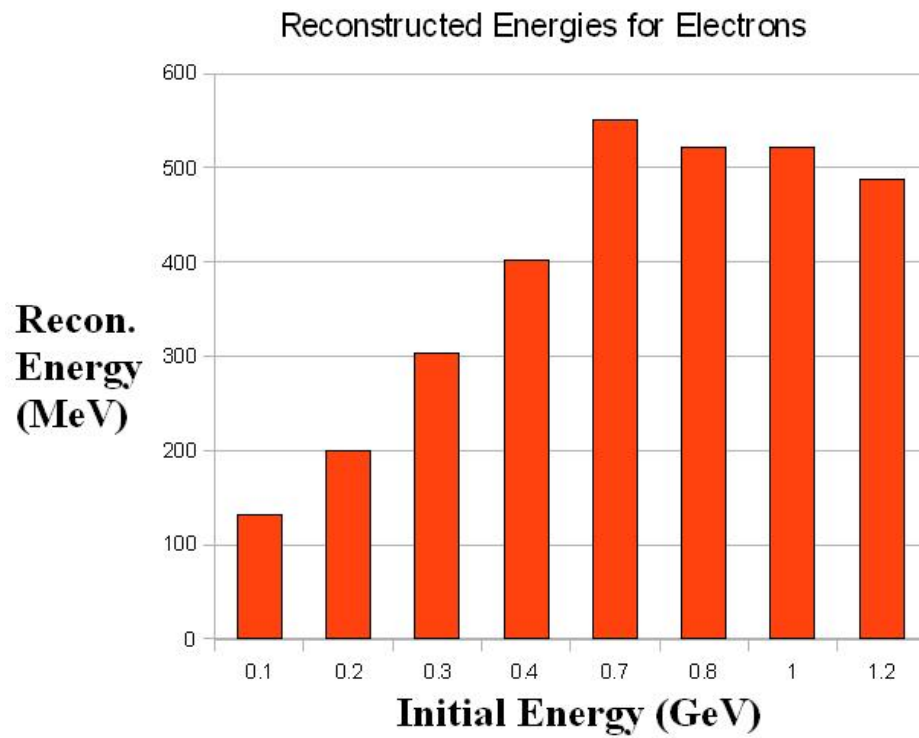
Figure 20: Reconstructed values for the total energy deposited by electrons at various energies, obtained by combining the results in Figures 17 and 19.
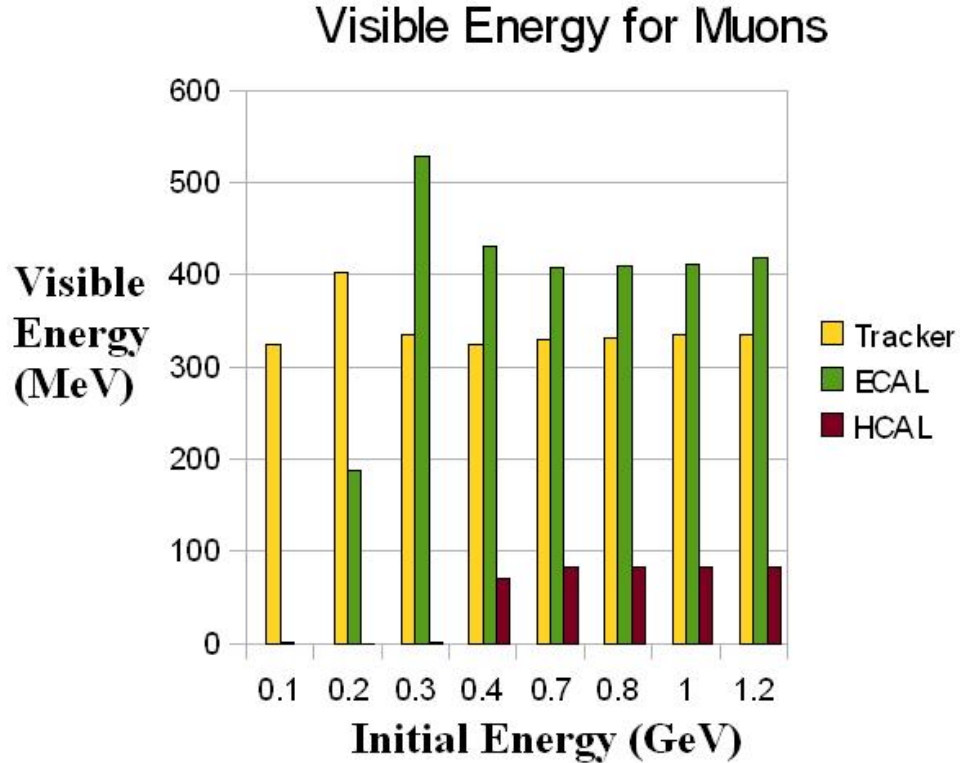
Figure 21: Average amounts of visible energy in the tracker, ECAL, and HCAL regions of the MTest detector as deposited by incoming muons.

Again, I walked through the same steps with muons. In this case, it appeared reasonable to allow that C may be nonzero so long as the muons did not exit the detector entirely, thus maintaining the constraint on total energy containment. Average visible energy in the MTest detector for muons of various initial momenta is given in Figure 21, the coefficients calculated after three iterations are given in Figure 22, and the reconstructed energies are given in Figure 23.

Although the reconstructed energies in Figure 23 are accurate even up to 1.2 GeV, the plateau in the pattern of visible energies in Figure 21 suggests strongly that muons above 0.4 GeV are exiting out the rear of the MTest detector. For this reason, only coefficients obtained for lower momenta are truly trustworthy. In fact, it may be most useful only to consider A and B and only for initial energies of 0.3 GeV or less, since these muons appear not to penetrate the HCAL at all and thus give the best possible case for total energy containment.
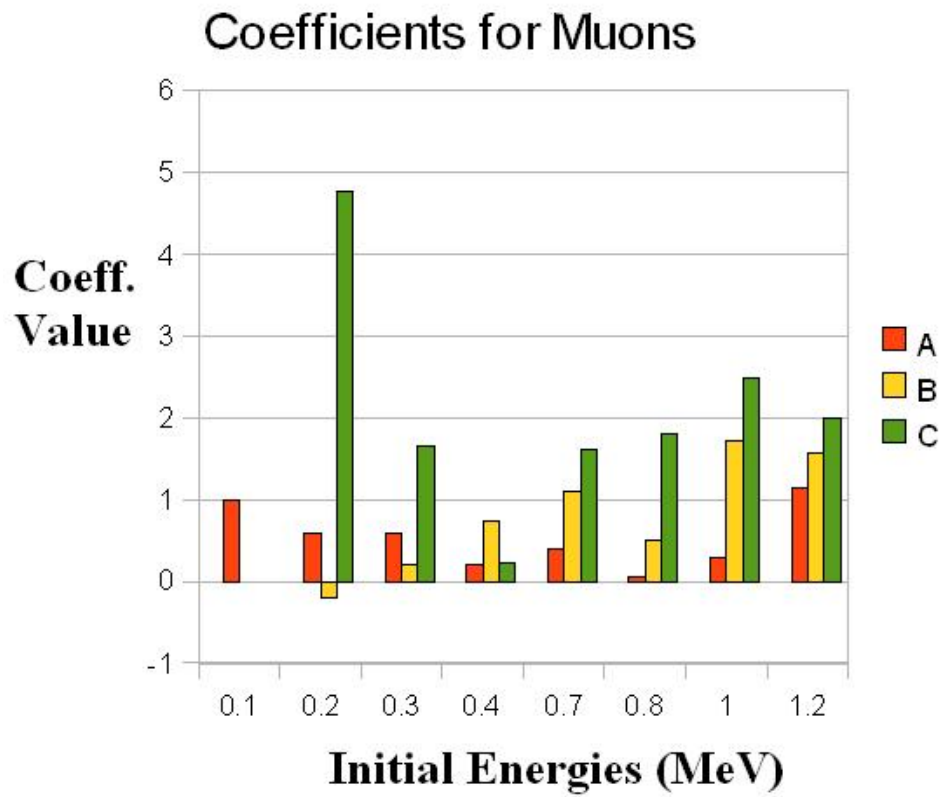
Figure 22: Final values for A_{muon}, B_{muon}, and C_{muon} at various energies after three iterations.
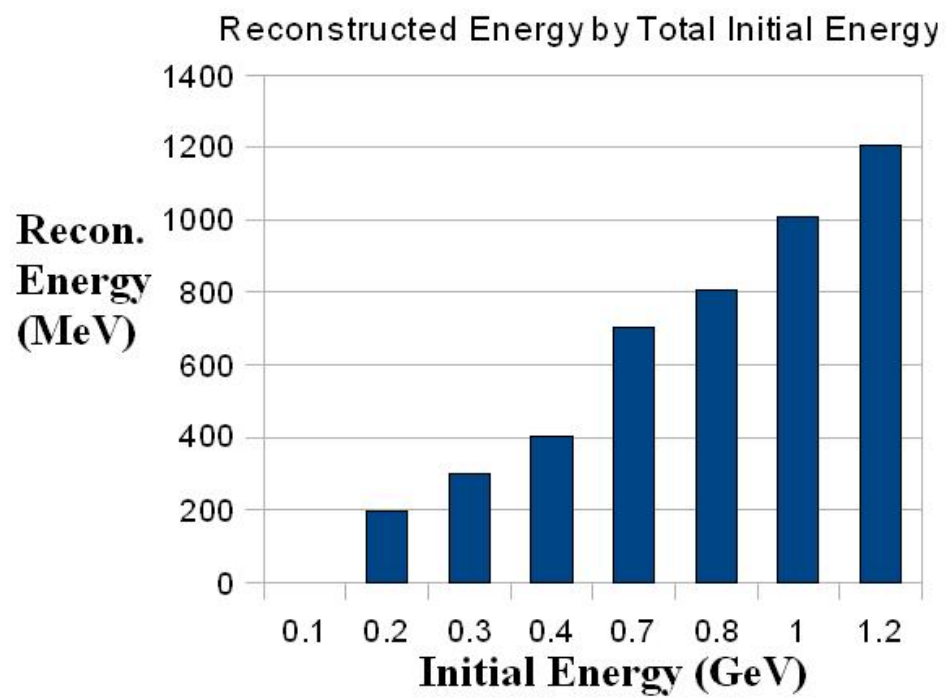
Figure 23: Reconstructed values for the total energy deposited by muons at various energies, obtained by combining the results in Figures 21 and 22.

To continue this investigation, many more samples must be analyzed for other particle types and energies. Specifically, I would inspect runs for each protons, electrons, muons, π^+, π^-, and π^0 at 0.1, 0.2, 0.3, 0.4, 0.7, 0.8, 1.0, and 1.2 GeV. These particles are the ones most frequently seen by MINERνA and the energies have been selected to sample the interesting features of the distribution of momenta carried by these particles when they are seen. A full survey of these particles and values would allow for the determination of any patterns in the relationship between each coefficient and each particle type and momentum.

8 Conclusions

Neutrinos and their oscillations are the subject-matter of some of the most exciting experiments in high-energy physics today. MINERνA represents a significant advancement of the global scientific knowledge base in this field. As the detector nears completion and MINERνA prepares to take large amounts of data, it is crucial that the researchers be prepared to handle and interpret that data. As a trained and certified scanner, I contribute to the preparedness of the Collaboration by discerning the critical features of neutrino interactions. These events are detected and characterized according to the energy deposition tracks left by the daughter particles and their subsequent interactions downstream. My work on MTest simulations represents an early contribution to the overall understanding of the data expected to be collected by the MINERνA detector.

References

[1] C. Amsler et al. (Particle Data Group). "The Review of Particle Physics : Neutrino Mass, Mixing, and Flavor Change." Physics Letters B 667: 1 (2008). http://pdg.lbl.gov/2008/reviews/rpp2008-rev-neutrino-mixing.pdf.

[2] "Didascalia ricciolo." Istituto nazionale di Fisica Nucleare - Sezione di Torino. Web. 15 Nov. 2009. http://oldsite.to.infn.it/activities/schedules/storia/Ricciolo-didascalia.htm.

[3] Frey, R. "Solar Neutrinos - Calculation of the Solar Neutrino Flux on Earth." Lecture. *Cosmic Ray Telescope Muon Detector"*. 23 Feb. 2006. Web. 22 Apr. 2010. ¡http://www.cosmicrays.org/muon-solar-neutrinos.php¿.

[4] Green, Dan. *The Physics of Particle Detectors* (Cambridge Monographs on Particle Physics, Nuclear Physics and Cosmology). New York: Cambridge UP, 2005. Print.

[5] Krane, Kenneth S., and David Halliday. "Section 9.6." *Introductory Nuclear Physics.* New York: Wiley, 1988. Print.

[6] MINERνA Collaboration, "The MINERνA Technical Design Report," MINERvA-doc-700-v28 (2006).

[7] Perkins, Donald H. *Introduction to high energy physics.* Cambridge: Cambridge UP, 2000. Print.

[8] Rene Brun and Fons Rademakers, *ROOT - An Object Oriented Data Analysis Framework*, Proceedings AIHENP'96 Workshop, Lausanne, Sep. 1996, Nucl. Inst. & Meth. in Phys. Res. A 389 (1997) 81-86. See also http://root.cern.ch/.